Appl. Magn. Reson. 26, 533–542 (2004)

Applied Magnetic Resonance

Electron Paramagnetic Resonance Study of Fe^{3+} Ions at Octahedral and Tetrahedral Mirror Symmetry Sites in the $LiScGeO_4$ Crystal

A. A. Galeev[1,2], N. M. Khasanova[1,2], C. Rudowicz[1], G. S. Shakurov[3], G. R. Bulka[2], N. M. Nizamutdinov[2], and V. M. Vinokurov[2]

[1] Department of Physics and Materials Science, City University of HK, Kowloon Tong, Hong Kong SAR
[2] Kazan State University, Kazan, Russian Federation
[3] Kazan Physical-Technical Institute, Russian Academy of Sciences, Kazan, Russian Federation

Received February 6, 2004

Abstract. An electron paramagnetic resonance (EPR) study of a synthetic single crystal of $LiScGeO_4$ doped with Cr ions carried out earlier at the X- and Q-bands at 300 K has indicated additional weak lines. A detailed analysis of these EPR lines, which were tentatively attributed to the Fe^{3+} ions at two different mirror symmetry sites, is presented in this paper. The angular dependences in the three crystallographic planes were resolved by fitting the two distinct spectra denoted Fe^{3+}(I) and Fe^{3+}(II) with a spin Hamiltonian ($S = 5/2$) of monoclinic symmetry. The rank-4 crystal field tensors at tetrahedral and octahedral sites were calculated with the point-charge model to determine the principal axis orientations of their cubic, tetragonal and trigonal components. A comparative analysis of the zero-field splitting tensors and the crystal field ones indicates that Fe^{3+}(I) ions substitute for Sc^{3+} at octahedral sites and Fe^{3+}(II) ions substitute for Ge^{4+} at tetrahedral sites with no significant distortion of the coordination polyhedra in the structure of $LiScGeO_4$.

1 Introduction

The structure of $LiScGeO_4$ belongs to the orthorhombic space group D_{2h}^{16} *Pnma* with $a = 1.0673$ nm, $b = 0.59926$ nm, $c = 0.49667$ nm [1]. Fe^{3+} ions in low concentrations are usual traces in the natural and synthetic crystals with olivine type structure thus determining their spectroscopic properties. In forsterite Mg_2SiO_4, Fe^{3+} ions were established as substituting at all the three structurally nonequivalent cationic sites [2, 3]: the octahedral M1 (4a) and M2 (4c) sites, and the tetrahedral (4c) sites. In chrysoberyl Al_2BeO_4, Fe^{3+} ions were established as substituting for Al^{3+} at the octahedral M2 site [4]. Previously we have reported [5] that in the Cr-doped crystal of $LiScGeO_4$, along with electron paramagnetic reso-

nance (EPR) spectra of Cr^{3+} at the Sc^{3+} sites, additional weak lines were observed. These EPR lines were tentatively attributed to the Fe^{3+} ions at two distinct mirror symmetry sites [5]. A detailed analysis of the two sets of lines denoted Fe^{3+}(I) and Fe^{3+}(II) is presented in this paper. This includes for each of the two substitutional sites Fe^{3+}(I) and Fe^{3+}(II) in $LiScGeO_4$:Cr (i) the experimental results and the fitted spin Hamiltonian (SH) parameters and (ii) detailed comparative analysis of the calculated rank-4 tensor for the zero-field splitting (ZFS) terms in SH as well as that for the crystal field (CF) terms and the respective crystallographic data.

2 Experimental Results

The main features of the X-, Q- and broad-band EPR spectra of the $LiScGeO_4$:Cr crystal under study were reported in ref. 5. Along with the most intense spectrum of Cr^{3+} ($S = 3/2$), additional weak spectral lines with no hyperfine satellites (Fig. 1) were observed at the X- and Q-bands. All these lines exhibit similar symmetry properties: any single spectral line is split into two lines when the external magnetic field deviates from the crystallographic *ab*- and *bc*-planes. In accordance with the space group D_{2h}^{16} *Pnma*, the observed spectral symmetry and the number of the magnetically conjugate spectra indicate that the paramagnetic ions responsible for these spectra occupy the 4c sites in the $LiScGeO_4$ structure [6]. To enable fitting SH parameters from the Q-band spectra, a representative number of experimental lines was collected from the spectral angular dependence in the three crystallographic planes (Fig. 2).

In order to resolve the observed spectra we use the SH ($S = 5/2$) [7, 8] of the Laue symmetry C_{2h} expressed in the axis system $x \| c$, $y \| a$ and $z \| b$, i.e.,

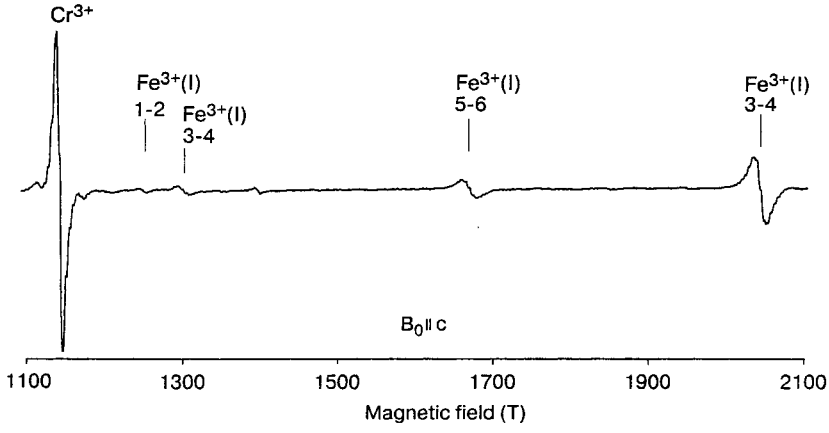

Fig. 1. Section of the X-band EPR spectrum of the Cr-doped $LiScGeO_4$ crystal at room temperature recorded on a PS100.X automated spectrometer. Transition lines of the Fe^{3+} centers are denoted by two numbers as indicated on the energy level diagrams in Fig. 3.

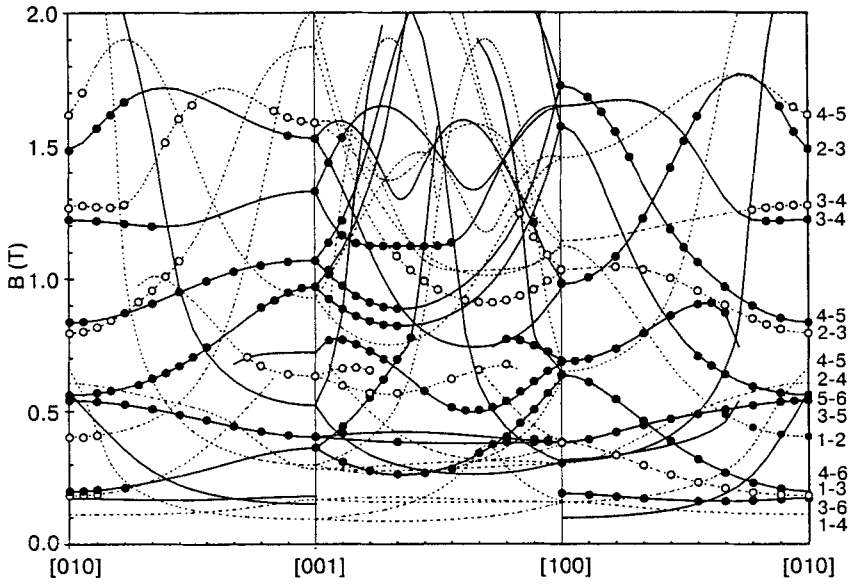

Fig. 2. Angular dependence of the Q-band EPR transitions for the Fe^{3+}(I) (filled circles, solid curves) and Fe^{3+}(II) (open circles, dashed curves) in $LiScGeO_4$:Cr crystal at room temperature in the three crystallographic planes. Circles denote the experimental data, whereas the curves are calculated with the SH parameters listed in Table 1. The two numbers on the right-hand side denote the transitions according to the energy level notation indicated in Fig. 3.

Table 1. SH parameters for Fe^{3+}(I) and Fe^{3+}(II) in $LiScGeO_4$:Cr (space group *Pnma*, $x \| c$, $y \| a$ and $z \| b$) at 300 K.

Parameter	Fe(I)	Fe(II)
g_{xx}	2.0032	2.0051
g_{yy}	2.0074	2.0072
g_{zz}	2.0050	2.0054
g_{xy}	0.0002	0.0025
B_{20} (b_2^0) (10^{-4} cm^{-1})	1874.95 (2296.3)	−2266.75 (−2776.2)
B_{22} (b_2^2) (10^{-4} cm^{-1})	815.16 (2445.5)	991.60 (2974.8)
B_{2-2} (b_2^{-2}) (10^{-4} cm^{-1})	1660.05 (4980.2)	1402.72 (4208.2)
B_{40} (b_4^0) (10^{-4} cm^{-1})	0.21 (0.77)	−2.05 (−7.37)
B_{42} (b_4^2) (10^{-4} cm^{-1})	3.32 (75.49)	1.73 (39.12)
B_{4-2} (b_4^{-2}) (10^{-4} cm^{-1})	8.64 (−196.00)	3.69 (83.66)
B_{44} (b_4^4) (10^{-4} cm^{-1})	−2.16 (64.92)	−4.42 (−132.60)
B_{4-4} (b_4^{-4}) (10^{-4} cm^{-1})	4.70 (−141.09)	2.04 (61.32)
N	117	69
ε (mT)*	1.92	1.10

* $\varepsilon = \left(\sum_{i=1}^{N} \Delta B_i^2 / (N-p)\right)^{1/2}$ value is the root-mean-square deviation of the measured and the computed resonance fields obtained for a fit of $p = 12$ parameters over N transitions involved.

Table 2. Principal axis systems and principal values of the SH tensors and MIC(O_h) for B_4 for Fe^{3+}(I) and Fe^{3+}(II). B_{2M} are in the units of 10^{-4} cm^{-1}; $S_4(O_h)$ are in the units of 10^{-8} cm^{-2}; angles are in degrees; the reference system relative to which the Euler rotations are given is $x \| c$, $y \| a$ and $z \| b$.

Tensor	Fe(I)		Fe(II)	
	Euler angles	Principal values	Euler angles	Principal values
g	$\alpha = 88.06$	$g_{xx} = 2.0050$	$\alpha = 56.25$	$g_{xx} = 2.0054$
	$\beta = 90$	$g_{yy} = 2.0032$	$\beta = 90$	$g_{yy} = 2.0034$
	$\gamma = 0$	$g_{zz} = 2.0074$	$\gamma = 0$	$g_{zz} = 2.0088$
B_2	$\alpha = 58.08$	$B_{20} = -3202.6$	$\alpha = 152.63$	$B_{20} = 3237.27$
	$\beta = 90$	$B_{22} = -223.5$	$\beta = 90$	$B_{22} = 529.23$
	$\gamma = 90$	$B_{22}/B_{20} = 0.07$	$\gamma = 90$	$B_{22}/B_{20} = 0.16$
$B_4(O_h)$	$\alpha = 58.76$	$S_4 = 225.2$	$\alpha = 127.09$	$S_4 = 84.8$
	$\beta = 90$	$S_4(O_h) = 212.0$	$\beta = 90$	$S_4(O_h) = 73.2$
	$\gamma = 45$	$d_4(O_h) = 0.058$	$\gamma = 45$	$d_4(O_h) = 0.14$

with the z-axis normal to the ac-plane which defines the monoclinic direction in the $LiScGeO_4$ crystal [5, 9]

$$\mathcal{H} = \mu_B(B_x g_{xx} S_x + B_y g_{yy} S_y + B_z g_{zz} S_z + B_x g_{xy} S_y) + B_{20}\bar{T}_{20} + B_{22}\bar{T}_{22} + B_{2-2}\bar{T}_{2-2} + B_{40}\bar{T}_{40} + B_{42}\bar{T}_{42} + B_{44}\bar{T}_{44} + B_{4-4}\bar{T}_{4-4}. \quad (1)$$

The details of the operators and parameters notation used in Eq. (1) can be found in ref. 5. All SH parameters for both Fe^{3+}(I) and Fe^{3+}(II) paramagnetic centers listed in Table 1 were obtained by fitting the spectral angular dependence in the three xy, xz and yz crystallographic planes with the modified program [10]. In the xyz axis system the parameters describing the symmetry-related spectra differ only in the sign of g_{xy}, B_{2-2}, B_{4-2}, and B_{4-4} from those given in Table 1, whereas the principal axis systems for the corresponding tensors are determined by Euler rotations $(\pi - \alpha, \beta, \gamma)$ with the values of α, β, and γ given in Table 2. To facilitate the comparison with other experimental data, the ZFS parameters in Table 1 are also given in the extended Stevens (ES) notation b_k^q [7]. The two ZFS within the three Kramers doublets of the spin $S = 5/2$ states were calculated from the SH parameters as $\Delta_1 = 1.54177$ cm^{-1} and $\Delta_2 = 0.83140$ cm^{-1} for Fe^{3+}(I) and as $\Delta_1 = 0.92458$ cm^{-1} and $\Delta_2 = 1.53669$ cm^{-1} for Fe^{3+}(II). The absolute signs of ZFS parameters were not determined experimentally, but the positive sign of B_{40} in the principal axis system for the maximum invariant component (MIC) of the cubic symmetry was chosen for each observed Fe^{3+} center to conform with the microscopic SH theory and experimental results for the tetrahedrally and octahedrally coordinated ^6S-state ions in other similar compounds [11–13]. The energy level diagrams together with the energy difference plots are presented in Fig. 3 for each Fe^{3+} center.

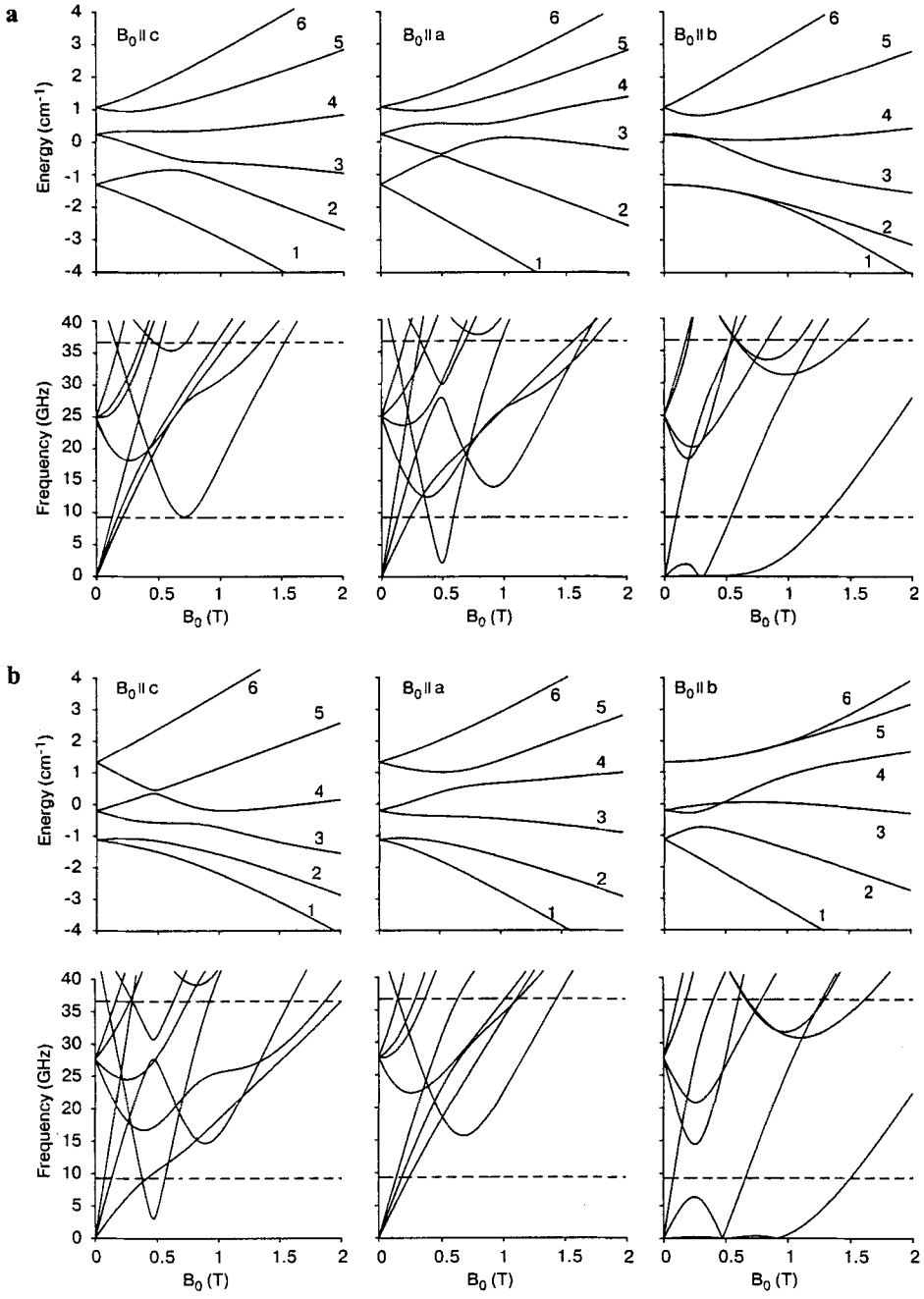

Fig. 3. Energy level and resonance frequency diagrams for the Fe^{3+}(I) (**a**) and Fe^{3+}(II) (**b**) in $LiScGeO_4$:Cr with the magnetic field B_0 along the crystallographic axes. For convenience, the numbers from 1 to 6 in the order of increasing energy denote the states. Dashed lines in the frequency diagrams indicate the two resonance frequencies used in this study.

3 Analysis of the SH Tensors and the CF Tensors

Table 1 shows that the diagonal values of the g-tensors for both Fe^{3+} sites have a positive deviation from the free-spin value and are within the range typical for Fe^{3+} in other compounds [12, 14]. A simple mean of the diagonal g_{ii} values for Fe^{3+}(II) is a little larger than that for Fe^{3+}(I). The ZFS and the spectrum anisotropy are mainly determined by the relatively large values of the rank-2 ZFS parameters for both centers, which are of the same order of magnitude as for Fe^{3+} ions at the mirror symmetry sites in forsterite [2] and chrysoberyl [4]. In the principal axis system of the rank-2 ZFS tensor chosen to satisfy the orthorhombic standardization [15, 16] yields the rhombicity ratio $B_{22}/B_{20} = 0.07$ for Fe^{3+}(I), which is close to the value of 0.06 [2] and 0.022 [4] for Fe^{3+} at the octahedral 4c sites in forsterite and chrysoberyl, respectively. A larger rhombicity ratio for Fe^{3+}(II) $B_{22}/B_{20} = 0.16$ compares well with that for Fe^{3+} at the tetrahedral Si sites in forsterite $B_{22}/B_{20} = 0.26$.

The most general invariant characteristic for the rank-4 ZFS tensor is a value of the rotational invariant S_4 defined as [8]

$$S_4 = (B_{40})^2 + 2 \cdot \sum_{M=1}^{4} ((B_{4M})^2 + (B_{4-M})^2) . \tag{2}$$

Oxygen-coordinated Fe^{3+} ions at the octahedral sites exhibit distinctly larger values of S_4 [17]. The value of S_4 for Fe^{3+}(I) in Table 1 is about three times larger than that for Fe^{3+}(II) and implies the validity of the assignment of Fe^{3+}(I) and Fe^{3+}(II) in $LiScGeO_4$:Cr to the octahedral and tetrahedral sites, respectively.

For a more detailed consideration of the structural peculiarities at the substitution sites we apply the methods of topological comparison (i.e., pseudosymmetry [18]) of the rank-4 ZFS tensors B_4 and the rank-4 CF tensors $[V_4 \otimes V_4] \equiv V_4^{44}$. The CF tensors were calculated with the point-charge model on the basis of the tesseral harmonics [13] and the crystallographic data [1]

$$V_{LM} = \sqrt{\frac{(L-M)!}{(L+M)!}} \sum_{j=1}^{N} \frac{q_j}{R_j^{L+1}} P_L^M(\cos\vartheta_j) \cdot \cos M\varphi_j ,$$

$$V_{L-M} = \sqrt{\frac{(L-M)!}{(L+M)!}} \sum_{j=1}^{N} \frac{q_j}{R_j^{L+1}} P_L^M(\cos\vartheta_j) \cdot \sin M\varphi_j , \tag{3}$$

where R_j, ϑ_j, and φ_j are polar coordinates of the charges q_j around the given transition ion. Note that there is a misprint in eq. (4) in ref. 13 for the CF tensors, which should be replaced by Eq. (3) above. For comparison we use the orientations of the principal axes for the MIC of the three possible symmetry groups G_s (i.e., $G_s = O_h$, C_{3i} and C_{4i}) and the distortion coefficients $d_4(G_s) = [S_4 - S_4(G_s)]/S_4$ in the principal axis system for MIC of symmetry G_s, which measures the departure of the tensors from the exact form for a given group G_s [8, 18].

Table 3. The bond directions in the [ScO_6] octahedron and [GeO_4] tetrahedron, orientations of the principal axes and the distortion coefficients $d_4(G_s)$ of MIC of symmetry $G_s = C_{3i}$ and C_{4i} for the tensor B_4 (SH) fitted for Fe^{3+}(I) and Fe^{3+}(II) and the tensor V_4^{44} (CF) calculated at the Sc^{3+} site in $LiScGeO_4$:Cr crystal; angles are in degrees.

Polyhedron	Bonds				G_s	B_4			V_4^{44}		
	Me-O	α	β	R (nm)		α	β	$d_4(G_s)$	α	β	$d_4(G_s)$
[ScO_6]	Sc-O2	61.95	90	0.20698	$C_{4i}(1)$	59.06	90	0.03	59.55	90	0.004
	Sc-O3	151.21	36.21	0.20801	$C_{4i}(2)$	148.94	45.22	0.05	149.55	44.98	0.005
	Sc-O3′	151.21	143.79	0.20801	$C_{4i}(3)$	148.94	134.78	0.05	149.55	135.02	0.005
					$C_{3i}(1)$	3.76	90	0.026	4.8	90	0.003
					$C_{3i}(2)$	113.57	90	0.06	114.26	90	0.005
					$C_{3i}(3)$	58.3	35.56	0.05	59.54	35.28	0.004
					$C_{3i}(4)$	58.3	144.44	0.05	59.54	144.72	0.004
[GeO_4]	Ge-O1	2.56	90	0.17325	$C_{3i}(1)$	0	90	0.10	0	90	0.19
	Ge-O2	65.22	90	0.17335	$C_{3i}(2)$	72.98	90	0.13	70.18	90	0.26
	Ge-O3	132.16	42.17	0.17784	$C_{3i}(3)$	128.14	36.06	0.10	129.02	38.42	0.19
	Ge-O3′	132.16	137.83	0.17784	$C_{3i}(4)$	128.14	143.94	0.10	129.02	141.58	0.19
					$C_{4i}(1)$	127.35	90	0.11	125.7	90	0.26
					$C_{4i}(2)$	37.24	44.2	0.13	35.67	44.95	0.26
					$C_{4i}(3)$	37.24	135.58	0.13	35.67	135.05	0.26

The orientations of the cubic axis system and distortion coefficients $d_4(O_h)$ of MIC of symmetry $G_s = O_h$ for the ZFS tensors B_4 are presented in Table 2. V_4^{44} calculated at the Sc^{3+} site with the coordinates (0.27151, 0.25, 0.00292) is characterized by the orientation of cubic axes given by the Euler angles $\alpha = 59.53°$, $\beta = 90°$, $\gamma = 45°$ and the distortion coefficient $d_4(O_h) = 0.02$. These values are close to the corresponding ones for B_4(ZFS) for Fe^{3+}(I) given in Table 2. For V_4^{44} calculated at the Ge^{4+} site with the coordinates (0.0901, 0.25, 0.4474) the minimum of $d_4(O_h) = 0.11$ is obtained in the cubic axis system given by $\alpha = 125.67°$, $\beta = 90°$, $\gamma = 45°$. These values are close to those for B_4(ZFS) for Fe^{3+}(II) in Table 2.

The orientations of the principal axes for the MIC of symmetry $G_s = C_{3i}$ and C_{4i} were calculated for both tensors B_4 and V_4^{44} in Table 3 to enable comparison of the MIC axes with the bond directions at the substitution sites in the $LiScGeO_4$ structure (Fig. 4). Due to the dominant cubic components in these tensors, there are four trigonal and three fourfold MIC axes, each closely corresponding to the symmetry axes of their respective cubic components. The results (Table 3) indicate a good match between the MIC axes of the B_4 tensor for Fe^{3+}(I) and those of V_4^{44} for the $[ScO_6]$ octahedron for both cases $G_s = C_{3i}$ and C_{4i}. The differences in their orientations do not exceed 1.3°. The tensors are also characterized by a slight variation in relatively small values of their distortion coefficients. For Fe^{3+}(I) the orientation of the least distorted fourfold axis in the symmetry plane ($d_4(C_{4i}) = 0.03$) is close to the principal z-axis of the B_2 tensor (discrepancy is less than 1°) and to the shortest bond Sc-O2 with the polar angles $\alpha = 61.95°$, $\beta = 90°$. The small rhombicity of the rank-2 tensor for Fe^{3+}(I) may indicate that a common source produces a dominating axial contribution to both the rank-2 and rank-4 ZFS tensors. Note that the oxygen at the vertex (Sc-O2) in the $[ScO_6]$ octahedron is shared with both the $[LiO_6]$ octahedron and the $[GeO_4]$ tetrahedron in the $LiScGeO_4$ structure. Similar relative orientations of the principal axes

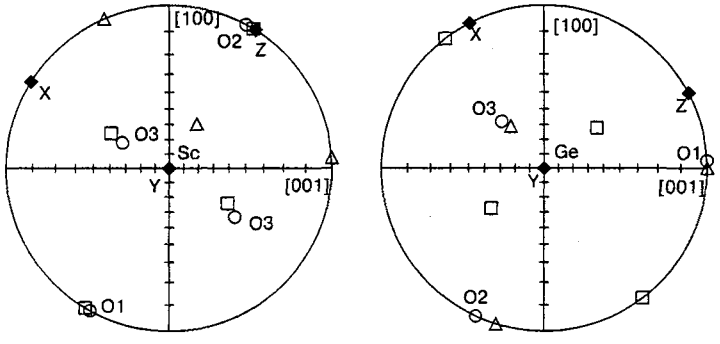

Fig. 4. Stereographic projection of the principal axes and bonds orientations for Fe^{3+}(I) at Sc site and Fe^{3+}(II) at Ge site. Open circles, the Me-O bonds; triangles, the principal axes of MIC(C_{3i}) for tensor B_4; open squares, the principal axes of MIC(C_{4i}) for tensor B_4; filled squares, principal axes for tensor B_2.

of the rank-2 and the rank-4 ZFS tensors are observed for the Fe^{3+}(M2) substituting for Mg^{2+} in forsterite [2], where the charge difference between the substituting ions may be responsible for an additional distortion and a larger deviation of these principal axes (discrepancy of about 4.2°).

The distortion coefficients in Table 2 characterizing the rank-4 tensors B_4 for Fe^{3+}(II) and V_4^{44} for $[GeO_4]$ are of the same order of magnitude and relatively large in comparison with those for Fe^{3+}(I) and $[ScO_6]$. The orientations of the MIC principal axes of both tensors are close to each other and the maximum difference of 2.8° is observed between the most distorted trigonal axis $C_{3i}(2)$, which is close to the bond Ge-O2 (the polar angles $\alpha = 65.22°$, $\beta = 90°$) with an oxygen shared by both the $[LiO_6]$ and $[ScO_6]$ octahedra in the structure. The relatively larger distortions of the rank-2 and rank-4 ZFS tensors for Fe^{3+}(II) as compared with those for Fe^{3+}(I) in $LiScGeO_4$ have also been observed for the ZFS tensors for the Fe^{3+} at $[SiO_4]$ site as compared with those for the M2 site in forsterite [2].

4 Conclusions

The EPR study of a single crystal of Cr-doped $LiScGeO_4$ at the X- and Q-bands and a comprehensive analysis of the fitted SH parameters allowed us to identify the additional weak lines observed in the spectra as originating from the Fe^{3+} ($S = 5/2$) ions substituting for Sc^{3+} and Ge^{4+}. The higher intensity of the spectral lines observed for Fe^{3+}(I) as compared with Fe^{3+}(II) indicates that Fe^{3+} ions preferably substitute for Sc^{3+} at the octahedral sites in this crystal. A heterovalent substitution of Fe^{3+} ions for Ge^{4+} at the tetrahedral sites occurs with no significant distortion of the coordination tetrahedron thus indicating that there is no additional charge-compensating ion in the nearest environment.

The main features of the SH tensors for Fe^{3+} ions compare well with those previously reported in the EPR studies of Fe^{3+} in forsterite [2] and chrysoberyl [4] having the same olivine type crystal structure. The rotational invariants S_4 of the rank-4 ZFS tensors for Fe^{3+} at the octahedral sites are relatively small ($219 \cdot 10^{-8}$ cm^{-2} in forsterite and $225 \cdot 10^{-8}$ cm^{-2} in $LiScGeO_4$) as compared with those for the sixfold coordinated Fe^{3+} in many other compounds [17]. Fe^{3+} ions at the tetrahedral sites are characterized by relatively high values of S_4 ($127 \cdot 10^{-8}$ cm^{-2} in forsterite and $85 \cdot 10^{-8}$ cm^{-2} in $LiScGeO_4$) as compared with the values for similar tetrahedra in other compounds [17]. The calculated distortion coefficients $d_4(O_h)$ reveal that the tetrahedral sites are more distorted from an exact cubic symmetry than the octahedral sites in the two crystals.

The principal values of the rank-2 ZFS tensors for Fe^{3+} at the octahedral 4c sites in $LiScGeO_4$, forsterite [2], and chrysoberyl [4] are negative and characterized by a small rhombicity. The principal values of the rank-2 ZFS tensors for Fe^{3+} at the tetrahedral sites in $LiScGeO_4$ (Table 2) and forsterite [2] have opposite signs and are characterized by a larger rhombicity. The tensors noticeably differ in the orientation of their principal axis systems, but the ZFS of the ground state energy levels remain of the same order of magnitude in the two crystals.

The comparative analysis indicates that SH parameters for Fe^{3+} ions in the crystals with olivine type structure reveal more similarities due to the common features of the same structural sites than differences which could be expected judging by the different valence of the substituting ions.

Acknowledgements

This work was supported by the RGC and the City University of Hong Kong through the research grant SRG 7000965.

References

1. Genkina E.A., Timofeeva V.A., Bykov A.B.: Zh. Strukt. Khim. **27**, 167–168 (1986)
2. Gaite J.M., Hafner S.S.: J. Chem. Phys. **80**, 2747–2751 (1984)
3. Gaite J.M., Rager H.: J. Phys. Condens. Matter **9**, 10033–10039 (1997)
4. Vinokurov V.M., Zaripov M.M., Stepanov V.G., Pol'skii Yu.E., Chirkin G.K., Shekun L.Ya.: Sov. Phys. Solid State **3**, 1797–1800 (1962)
5. Galeev A.A., Khasanova N.M., Rudowicz C., Shakurov G.S., Bykov A.B., Bulka G.R., Nizamutdinov N.M., Vinokurov V.M.: J. Phys. Condens. Matter **12**, 4465–4473 (2000)
6. Nizamutdinov N.M., Bulka G.R., Gainullina N.M., Vinokurov V.M. in: The Physical Properties of Minerals and Rocks (Vinokurov V.M., ed.), pp. 3–48. Kazan: Kazan State University Press 1976.
7. Rudowicz C.: Magn. Reson. Rev. **13**, 1–89 (1987); Magn. Reson. Rev. **13**, 335–335 (1988)
8. Khasanova N.M., Nizamutdinov N.M., Vinokurov V.M., Bulka G.R.: Sov. Phys. Crystallogr. **33**, 527–533 (1988)
9. Rudowicz C. in: Proceedings of the International Conference on Spectroscopy, X-Ray and Crystal Chemistry of Minerals (Bakhtin A., ed.), pp. 31–41. Kazan: Kazan University Press 1998.
10. Bacquet G., Dugas J., Escribe C., Gaite J.M., Michoulier J.: J. Phys. C: **7**, 1551–1563 (1974)
11. Watanabe H.: Phys. Rev. Lett. **4**, 410–411 (1960)
12. Galeev A.A., Khasanova N.M., Bykov A.V., Bulka G.R., Vinokurov V.M., Nizamutdinov N.M.: Appl. Magn. Reson. **11**, 61–86 (1996)
13. Vinokurov V.M., Al-Soufi A.R., Galeev A.A., Khasanova N.M., Bulka G.R., Nizamutdinov N. M.: Appl. Magn. Reson. **7**, 323–327 (1994)
14. Abragam A., Bleaney B.: Electron Paramagnetic Resonance of Transition Ions, pp. 436–446. New York: Dover 1986.
15. Rudowicz C., Bramley R.: J. Chem. Phys. **83**, 5192–5197 (1985)
16. Rudowicz C., Madhu S.B., Khasanova N.M., Galeev A.: J. Magn. Magn. Mater. **231**, 146–156 (2001)
17. Vinokurov V.M., Gaite J.M., Bulka G.R., Khasanova N.M., Nizamutdinov N.M., Galeev A.A., Rudowicz C.: J. Magn. Reson. **155**, 57–63 (2002)
18. Michoulier J., Gaite J.M.: J. Chem. Phys. **56**, 5205–5213 (1972)

Authors' address: Akhmet A. Galeev, Kazan State University, 18 Kremlevskaya ulitsa, 420008 Kazan, Russian Federation
E-mail: akhmet.galeev@ksu.ru